This document is downloaded from the
Digital Open Access Repository of VTT

Title	Surface-micromachined silicon air-gap Bragg reflector for thermal infrared
Author(s)	Tuohiniemi, Mikko; Blomberg, Martti
Citation	Journal of Micromechanics and Microengineering vol. 21:7, pp. Article number 075014.
Date	2011
URL	http://dx.doi.org/ 10.1088/0960-1317/21/7/075014
Rights	Copyright © (2011) IOP Publishing. Reprinted from Journal of Micromechanics and Microengineering. This article may be downloaded for personal use only

VTT
http://www.vtt.fi
P.O. box 1000
FI-02044 VTT
Finland

By using VTT Digital Open Access Repository you are bound by the following Terms & Conditions.

I have read and I understand the following statement:

This document is protected by copyright and other intellectual property rights, and duplication or sale of all or part of any of this document is not permitted, except duplication for research use or educational purposes in electronic or print form. You must obtain permission for any other use. Electronic or print copies may not be offered for sale.

Surface-micromachined silicon air-gap Bragg reflector for thermal infrared

M Tuohiniemi[1] **and M Blomberg**[2]

[1] VTT Technical Research Centre of Finland, P.O. Box 1000, FI-02044 VTT
[2] VTT Memsfab Ltd, P.O. Box 1000, FI-02044 VTT

E-mail: mikko.tuohiniemi@vtt.fi

Abstract
We present a MEMS-based distributed Bragg reflector for thermal infrared (TIR) wavelengths 7 µm < λ < 12 µm. Surface micro-machining process flow was developed for [poly-Si / air-gap / poly-Si] λ/4-mirror using LPCVD SiO_2 as intra-mirror and mirror-to-substrate sacrificial layers. Circular 3-mm-diameter mirrors with theoretical reflectance exceeding 99% were designed. Poly-Si layers of the mirror were anchored for retaining constant mutual distance. Anchoring density and mirror-to-substrate gap were varied among samples.
We utilized scanning-electron microscope (SEM) imaging for qualitative estimation of processing result success as well as for layer-thickness measurements. We characterized the mirrors topography and mechanical response under local point loading by scanning with a stylus profilometer. Fourier-transform IR (FT-IR) spectroscopy was utilized in studies of reflectance spectrum. A one-dimensional computer simulation was allowed to fit model parameters to FT-IR data. Best-fit thicknesses of air-gaps and poly-Si layers were compared with design parameters and with SEM measurements in order to verify the final structure corresponded to the design.

1. Introduction

Exploiting micro-opto-electro-mechanical systems (MOEMS) technology at thermal-infrared (TIR) regime is inherently attractive leaving the typical structural dimensions well below the wavelength. Standard lithography and etching techniques readily produce few-micron features almost invisible to 10-µm waves. Optical surface flatness of layers deposited is guaranteed. MOEMS layout and process design for TIR benefits from a freedom of choice whether structural members of the system should interfere with the radiation or not.
The limited selection of well established MEMS materials is further reduced where transparency at TIR is mandatory. The device targeted in the current study, a quarter-wave distributed Bragg reflector (λ/4 mirror) [1], necessarily requires two transparent layers exhibiting sufficiently different refractive indices, i.e., good mutual contrast [2,3]. Besides low-conductivity silicon, only exotic solid materials [4] are available. A silicon air-gap λ/4 mirror thus appears a natural approach. Air-gap mirror is also in line with our next goal of realizing a voltage-controlled tuneable Fabry-Perot [5] interferometer (FPI) operating at TIR. The associated adjustable λ/2 cavity calls for the air gap anyway.
MEMS FPIs operating at shorter IR wavelengths below 5 µm are widely studied and published as reviewed in [6]. FPIs utilizing air-gap Bragg mirrors are published with InP [7-9] or Si_3N_4 [10] as the solid optical material and operating wavelengths near 1.5 µm. Lead salts have been speculated for extending MEMS Bragg mirror operation to λ = 30 µm [4]. Literature appearances of optical filters based on silicon with air gaps include a low-resolution MOEMS operating up to λ = 8 µm [11] and a non-MEMS solution [12] for

3µm < λ < 13µm. We have not found prior reports on MEMS air-gap Bragg mirror based on poly-Si thin films.
The mirror alone as presented in the current study is a very general component in terms of applicability because it provides wide operational wavelength range and high spectral reflectance. Applications of TIR-FPI emerge from variety of fields exploiting spectroscopy on organic compounds or polymers in gases or fluids. Presence of multiple substances, often H_2O, limits the spectral windows feasible for spectroscopic recognition. Accordingly, extension of available wave-length range into longer IR is called for.

2. Mirror design

General λ/4 mirror structure consists of alternating layers of quarter-wavelength (λ/4) optical thickness. Adjacent layers must exhibit sufficient contrast of the refractive-index $n(\lambda)$. Materials must also be transparent with the extinction coefficient $k(\lambda)$ remaining below 10^{-3}. Our three-layer λ/4 mirror structure is [poly-Si / air / poly-Si] featuring the associated contrast $n_{Si} : n_{AIR} = 3.42 : 1$ and $k < 2*10^{-4}$ at 5 µm < λ < 20 µm [13]. Released from the substrate by another λ/4 air gap, the theoretical reflectivity of the structure exceeds 99 % over a wide band of ca. 20 % of nominal λ. We targeted at λ = 9300 nm implying 2325-nm air gaps and 680-nm poly-Si layers.

The poly-Si layers were perforated with small holes (see figure 1) allowing wet-HF release etching of sacrificial SiO_2 layers. Hole diameters of 2 µm and 3 µm were tested. Poly-Si layers were anchored at constant vertical distance with 3-µm or 4-µm-wide plugs formed from the upper poly-Si layer. The 3-mm-diameter circular mirrors had 400 to 1600 anchors located to follow radial symmetry. Air gap between the mirror and the substrate was not anchored for better feasibility demonstration of a voltage-controllable FPI.

Poly-Si layers were adjusted at sufficient tensile stress state such that despite the anchors breaking the mirror-normal symmetry (anchor top open, bottom closed), the poly-Si layers remain planar given the anchors are small enough. Since our targeted future application, the FPI, calls for as-low-as-possible control voltage, too high a stress was also to be avoided and a compromise at 100 MPa was chosen.

A capacitively actuated mirror in an FPI eventually ends up pulled into a snap-in over the voltage-controlled air gap. In order to prepare for potential stiction issues, we also demonstrated an anti-stiction bump solution without any additional mask layers. Bumps extend from mirror bottom surface into the air gap below the mirror (see figure 2). Bumps can be designed at locations of anchors. Bump height can be anything below 2/3 of the controlled gap since only some 1/3 gap is in use until snap-in.

3. Fabrication process

The 150-mm substrate was a p-type doped single-side polished (SSP) single-crystalline silicon (sc-Si) wafer specified for 1-50 Ohm-cm resistivity. A low-pressure chemical-vapour deposited (LPCVD) SiO_2 was first deposited for mirror-to-substrate sacrificial layer. Next depositions were mirror lower poly-Si, intra-mirror sacrificial LPCVD SiO_2 and, mirror top poly-Si. Both poly-Si layers were individually annealed for proper stress state after deposited. The latter three layers were each patterned utilizing fluorine plasma for poly-Si and chlorine plasma etching for the oxide.

Processing-flow overview (see figure 1) illustrates a normal anchor and one forming an anti-stiction bump. Since all depositions are LPCVD processes, stress-balancing layer stack is also formed on the substrate back side.

A λ/4-gap both in and below the mirror would have done for demonstrating the TIR air-gap λ/4 mirror but, the inter-mirror air gap of an FPI must be over λ/2 thick. In order to demonstrate the feasibility, we also processed mirrors with a 5-µm air gap between the mirror and the substrate. The associated thick sacrificial oxide is challenged to stand over 900°C annealing without cracking during the poly-Si layer stress-state adjustment. A development effort of LPCVD SiO_2 deposition was involved to fulfil the requirements.

Fine tuning of layers final thickness to hit the nominal target was out of scope of the present study. Accordingly, as seen in table 1 below, the layers exhibited dimensions relatively far apart from λ/4 of any

single wavelength. Poly-Si layers ended up 650-680 nm and λ/4 sacrificial SiO_2 layers 2300-2600 nm thick. The deviation should not hinder the proof of concept since measured optical-performance data was compared with simulations based on realized layer thicknesses.

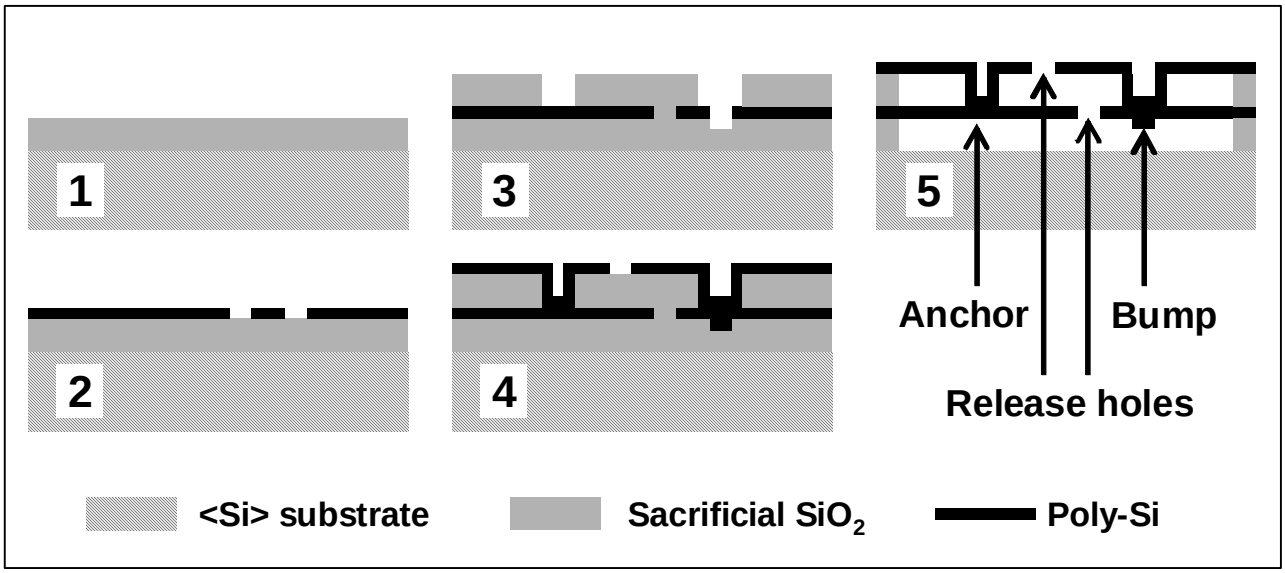

Figure 1. The device side of fabricated sample wafers is shown. 1) Mirror-to-substrate air-gap sacrificial LPCVD SiO_2 on <Si> substrate, 2) λ/4 mirror lower poly-Si layer, 3) Intra-mirror air-gap sacrificial LPCVD SiO_2, 4) λ/4 mirror upper poly-Si layer, 5) Wet-HF release etching.

4. Results and discussion

SEM image (see figure 2) gives a qualitative picture of sample fabrication result. Sample cleaving releases the poly-Si layers stress state but λ/4 mirror structure and anchoring idea are still well illustrated.

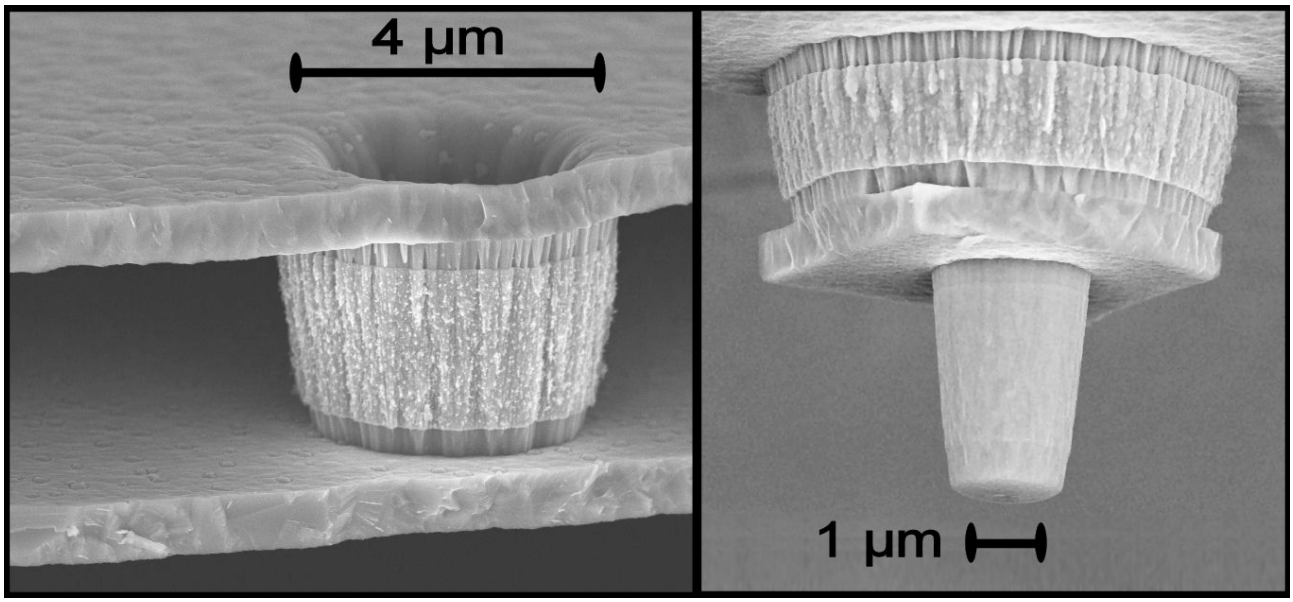

Figure 2. *Left*: The two poly-Si layers of the air-gap λ/4 mirror are shown with an anchor fixing the inter-layer distance after release etching. *Right*: An anti-sticktion bump extends into the mirror-to-substrate gap under the λ/4-gap anchor. Lower poly-Si layer is broken around the anchor.

SEM micrograph shows how the poly-Si surface is optically smooth for 7- to 12-µm wavelengths. The anchor is of wider type among those demonstrated. Identically performing 3-µm anchors brought their lateral

extent below λ/2 of the wavelengths of interest. The small fraction below 0.1 % of total mirror area occupied by the anchors in part ensures their harmlessness on optical performance.

4.1. Stylus profiling

Stylus profilometer Dektak 6M (by Veeco Instruments, Inc.) with 12-µm-diam tip was used for scanning the topography of the released mirrors surface. Evidently, the stylus force bends the mirror membrane during scanning. Two modes of bending are present: 1) The λ/4 mirror bends as a whole and, 2) the upper poly-Si layer alone bends. Scanning with different needle weights reveals the behaviour.

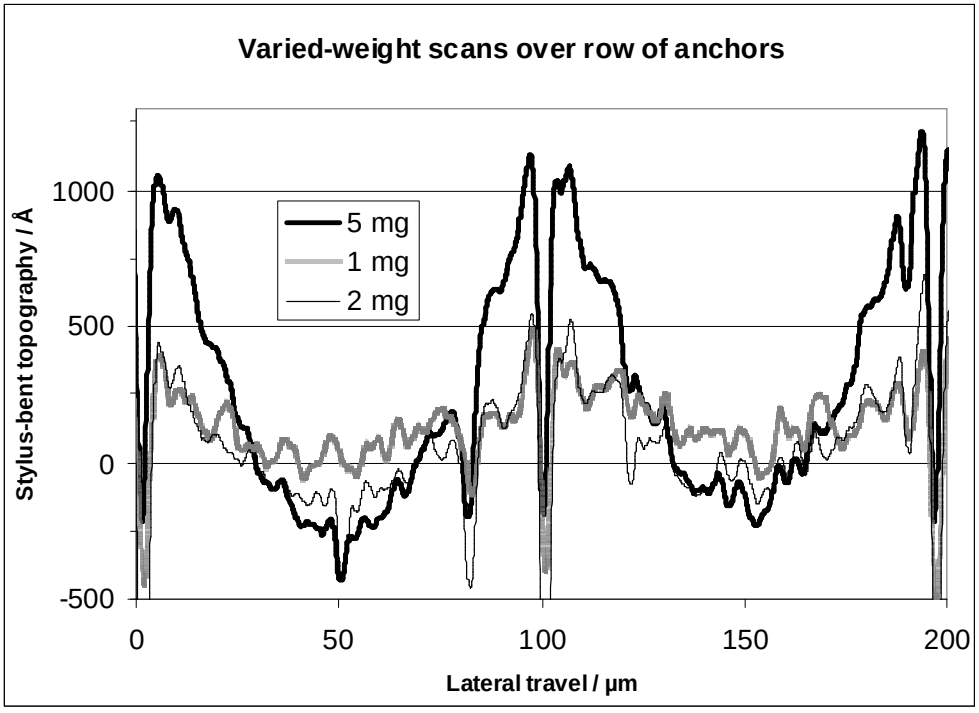

Figure 3. Short scans with stylus-weight varied. Adjacent anchors were crossed at 0, 100, and 200 µm. Pits at 50 µm and 80 µm are non-bulls-eye crossings of 3-µm-diam release holes.

200-µm scans (see figure 3) carefully targeted to cross 100-µm spaced anchors at the middle of membrane reveal the local inter-anchor behaviour of top poly-Si layer alone. Bending of 30 nm, 50 nm and, 150 nm are observed for stylus weights of 1 mg, 2 mg and 5 mg, respectively.

Mirror global bending as a whole was studied by scanning over the 3-mm diameter with 1-mg and 2-mg stylus weights. Mirror anchored at 400 points bends clearly deeper compared with a 1600-anchors design (see figure 4). Keeping in mind the stylus scan loads and records locally a point at a time, one must estimate the possibility of whole-mirror scan just passing all anchors at longer distance when scanning across the sparser-anchored version. However, the consistently 5-fold deeper long-scan bending taking gradually place over 1000-µm scan from edge towards middle cannot result from other phenomena than global bending. Maximal inter-anchor distance at wafer middle in the 400-anchor design is 150 µm to be compared with the 100-µm spacing studied in the 3-anchor scan (figure 3). Distance-square dependence [14] only explains (75/50)^2=2.25 times larger local bending so that more than another factor of two is due to mirror global bending.

The profiling results indicate that anchoring density provides a method for controlling the overall stiffness against bending in, e.g., a voltage-controlled application like the FPI. The FT-IR data below (figures 6 and 7) indicates sparser anchoring is safe in an application without any local point load present.

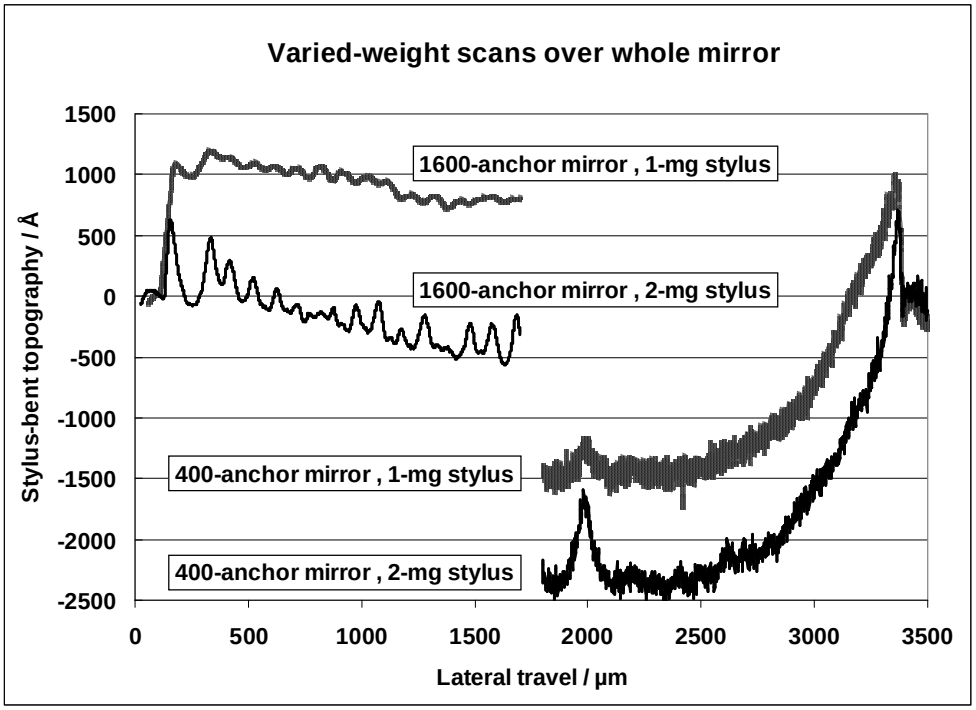

Figure 4. Longer scans over 3-mm mirrors with stylus-weight varied reveal the global bending as a function of anchoring density.

A distinctive feature in all stylus scans is the 100-nm rising of the surface over a 10-µm range at the mirror release-area edge (see figure 5). Underlying mechanism originates from the non-released sacrificial layer contacting the mirror periphery asymmetrically only from below. Potential moisture and temperature dependence of the phenomenon renders it harmful. Locally stiffening intra-mirror corrugation realized by the anchoring feature of the process flow has been speculated for eliminating the issue in future applications of the mirrors.

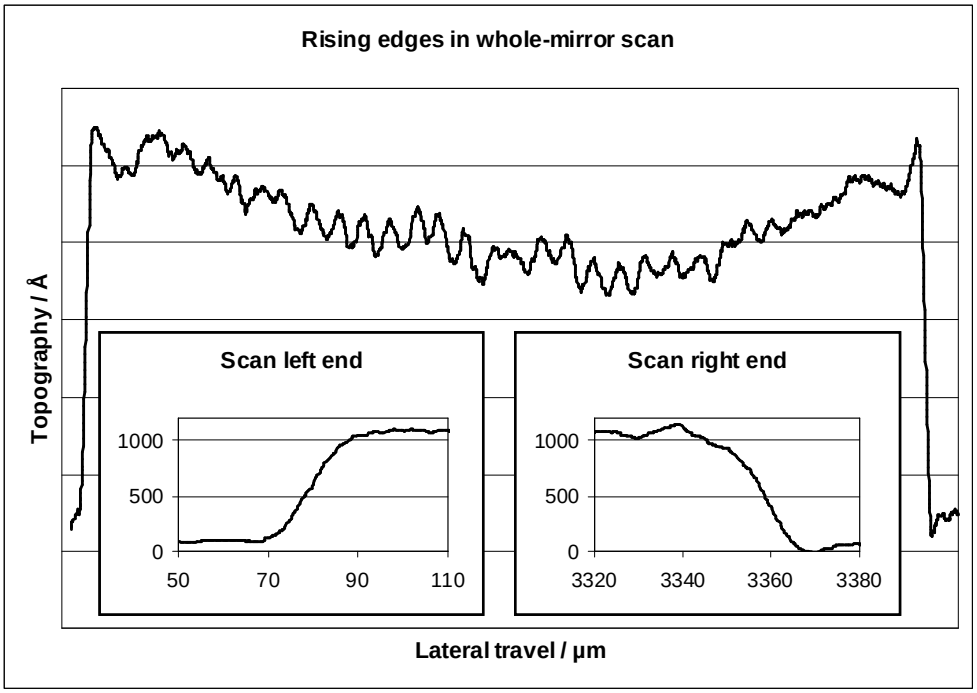

Figure 5. Lateral magnification of a whole-mirror stylus scan reveals the 100-nm up-lifting of mirror surface over some 10-µm range at mirror released-area edge.

4.2. FT-IR spectra

Our most descriptive method of characterizing the fabrication result were reflection measurements using Fourier-transform infrared (FT-IR) spectrometer (Bruker Vector22). Reflectance 100% reference was an Al-coated glass mirror. Sample was mounted on a focussing jig (by Harrick Scientific, Inc.) for 12-degree incident-angle reflection measurements. IR-beam was screened outside some half of mirror radius by poly-urethane sheet proven black below noise level (5% of signal) over the whole spectrum scanned (1500 nm < λ < 20000 nm). We reached some +/- 2% repeatability, estimated by comparing measurements of the same sample rotated around mirror normal.

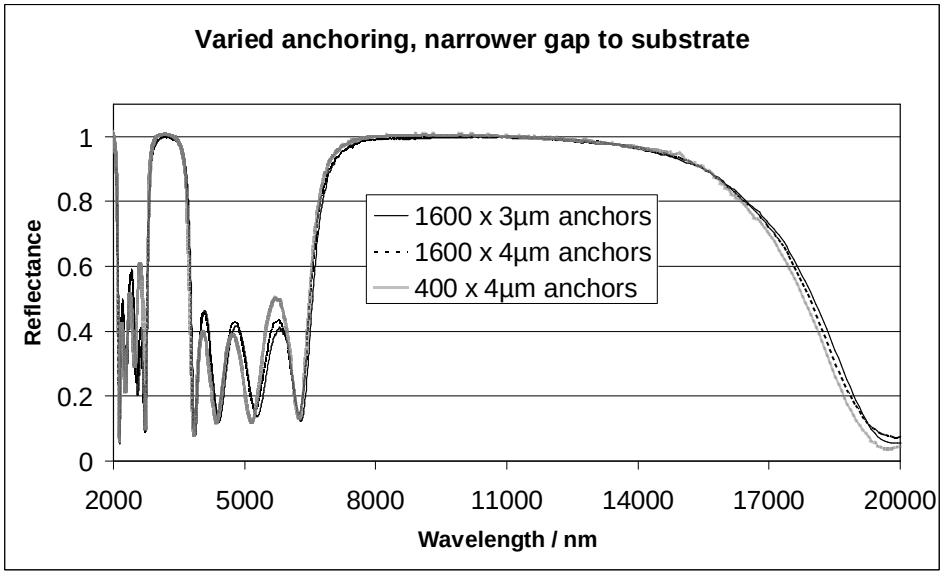

Figure 6. Reflection spectra of mirrors with varied anchoring. Nominal targeted substrate-to-mirror spacing was λ/4 = 2325 nm.

FT-IR scans of λ/4 mirrors with different sizes and densities of anchors (see figures 6 and 7) do not indicate any effect of the anchoring type on the reflection spectrum. The 2% repeatability tolerance affects the data in figure 7, where two curves actually exceed 100% reflectivity at λ=3050 nm but, one remains below 98%. Deviation from the predicted 99.1 % remains within measurement inaccuracy.

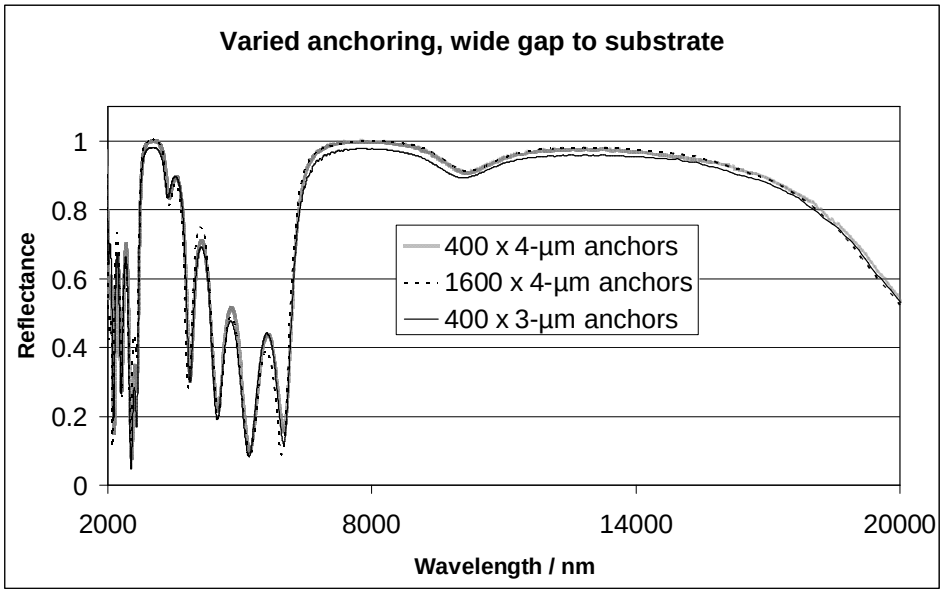

Figure 7. Reflection spectra of mirrors with varied anchoring. Nominal targeted substrate-to-mirror spacing was λ/2 = 4650 nm.

The measured reflection spectra were compared with one-dimensional simulations (TFCalc, Software Spectra, Inc.) A model was fitted with the data such that mirror air-gap and poly-Si layer thicknesses were allowed to vary. Samples back side was modelled with fixed layer thicknesses of SiO_2 and poly-Si based on SEM cross sections. Mirror air gaps and poly-Si thicknesses found by best fit were finally compared with those measured from SEM images.

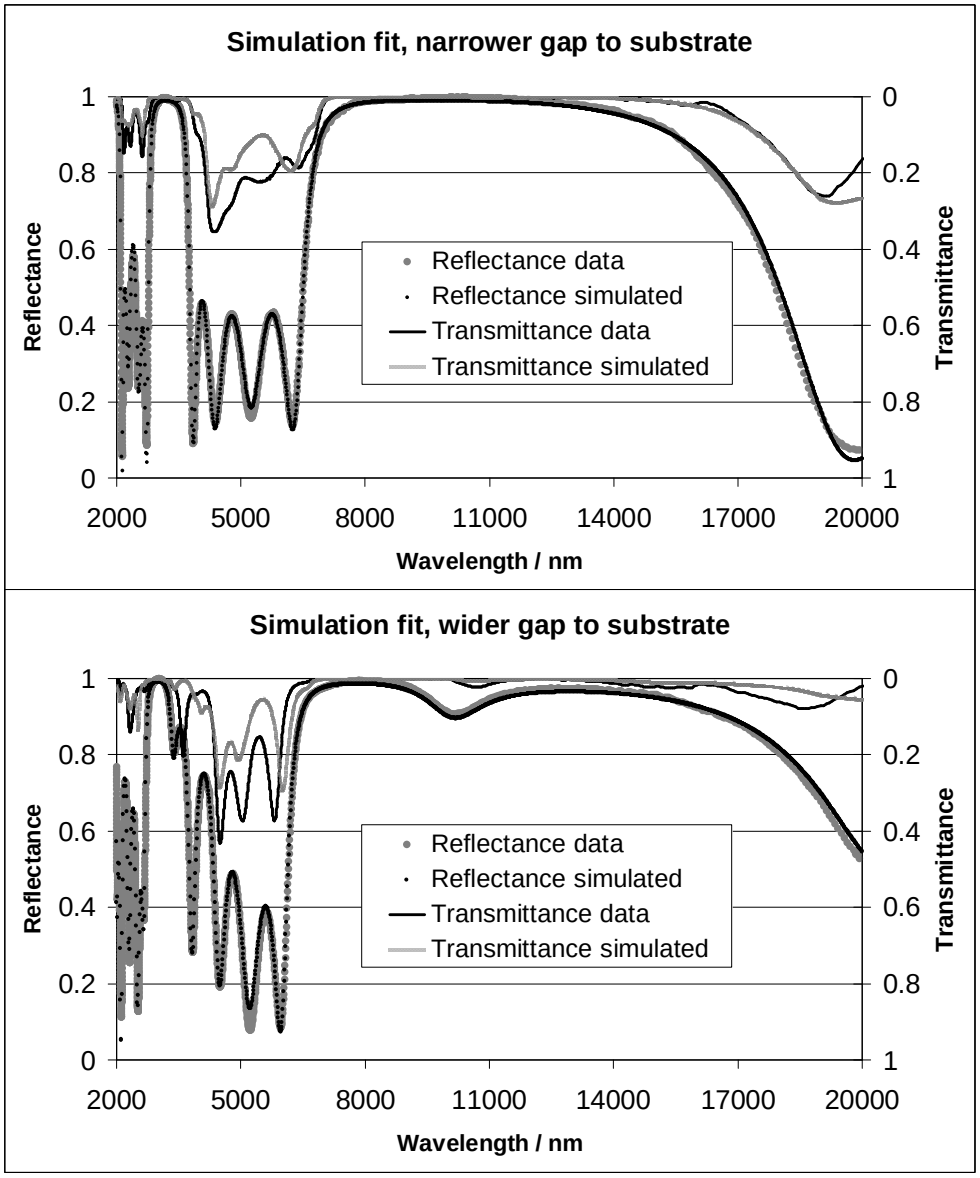

Figure 8. Mirror-samples reflectance and transmission spectra with simulation of model fitted with reflection data. The simulated transmission data is also shown.

For the mirror non-doped poly-Si layers, sc-Si data [13] for both $k(\lambda)$ and $n(\lambda)$ was considered adequate optical parameters in the simulation model. For the bulk sc-Si substrate, same data was used for $n(\lambda)$ but, $k(\lambda)$ was modelled differently as explained below.

Samples transmission spectra were also measured in order to estimate the substrate losses and the role of scattering at the non-polished back surface. A one-dimensional simulation being unable to count for optically rough surfaces and scattering, alternative means was applied for preventing the simulation from exaggerating back-surface reflection. The simulation-model substrate was adjusted for higher loss than reality so that

simulated transmission spectrum roughly matched the corresponding measurement data. The loss adjustment found optimal was a manual constant shift of extinction coefficient: $k_{MODEL} = k_{SC\text{-}Si}(\lambda) + 5*10^{-4}$.

Table 1. Layer thicknesses from SEM cross section images and from best fit of simulation model. All dimensions are given in nanometres. Blank entries remind that air-gaps were not directly measured whereas wafer back-side SiO_2 layers were not allowed to vary in simulation fit.

	Wider gap below mirror		Narrower gap below mirror	
	Simulated	Measured	Simulated	Measured
Lower Sacr SiO2	-	4910	-	2200
Air-gap below mirror	5280	-	2540	-
Intra-mirror Sacr SiO2	-	2320	-	2570
Intra-mirror λ/4 air gap	2320	-	2560	-
Mirror lower poly-Si	670	660	660	650
Mirror upper poly-Si	680	660	670	650

Simulated reflection spectra match that measured (see figure 8) indicating samples function as designed. All poly-Si layer thicknesses suggested by data fit (see table 1) match SEM measurement within 3 %. The perfect <0.5 % match of intra-mirror gap must be partly due luck since SEM-measurement reaching some 20-nm repeatability at its best already implies 1 % expected minimum variation. However, results clearly suggest the mirror structure follows that designed. The concept seems adequate for the purpose of realizing a MEMS FPI for thermal infrared.

Simulation fit suggests wider mirror-to-substrate air gap compared with corresponding sacrificial SiO_2 thickness. Near 350 nm uplift of the mirror is seen in the data consistently for both types of samples. Stylus-profilometer scans (see figure 5) already indicated the mirror is lift 100 nm farther from substrate over a 10-µm border of released area. The uphill seems to continue towards mirror centre but, due to stylus weight (minimum 1 mg), contact profiling cannot reveal the non-loaded situation. On the other hand, non-contact profiling by white-light interferometry was of no help due to interference effects at successive layer interfaces.

5. Summary

Air-gap poly-Si λ/4 mirrors were prepared and characterized for mechanical and optical performance. Poly-Si layers anchoring density seems to affect on the mirror stiffness against mechanical loading but not on the optical performance. Mirrors reflectance spectra were found to match the simulation result with model dimensions corresponding the reality. Simulation best fit on reflectance data well reproduced the mirror layers thicknesses determined from SEM cross-section images. Simulation fit suggests the mirror-to-substrate distance differ from that defined by corresponding sacrificial-layer thickness. The observation was partly supported by stylus-profiling results and thus accepted describing the real situation.

The study proved the concept of poly-Si/air λ/4 mirror as a basic building block enabling a tuneable FPI operating at 7 µm < λ < 12 µm. Certain development tasks were suggested. Sacrificial layers thickness must be better controlled and a deformation lifting the released mirror upwards must be minimized.

Acknowledgements

The work was in part funded by the Finnish Funding Agency for Technology and Innovation (TEKES): funding decision 40423/09. The authors wish to acknowledge Ms. Kirsi Järvi for precise work in sample-wafer processing.

References

[1] Turner A F and Baumeister P W 1966 Multilayer mirrors with high reflectance over an extended spectral region *Applied Optics* **5** 69

[2] Babic D I and Corzine S W 1992 Analytic Expressions for the Reflection Delay, Penetration Depth, and Absorptance of Quarter-Wave Dielectric Mirrors *IEEE J. of Quantum Electronics* **28** 514

[3] Brovelli L R and Keller U 1995 Simple Analytical Expressions for the Reflectivity and the Penetration Depth of a Bragg Mirror Between Arbitrary Media *Optics Communications* **116** 343

[4] Felder F, Fill M, Rahim M, Zogg H, Quack N, Blunier S and Dual J 2010 Lead Salt Resonant Cavity Enhanced Detector with MEMS Mirror *Physics Procedia* **3** 1127

[5] Born M and Wolf E 1959 (1993) *Principles of Optics, (6th ed. reprinted with corrections)* (Oxford, UK : Pergamon Press) p 329

[6] Schuler L P, Milne J S, Dell J M and Faraone L 2009 MEMS-based microspectrometer technologies for NIR and MIR wavelengths *J. of Physics* D - *Applied Physics* **42** art.no. 133001

[7] Le Dantec R, Benyattou T, Guillot G, Spisser A, Seassal C, Leclercq J-L, Viktorovitch P, Rondi D and Blondeau R 1999 Tunable Microcavity Based on InP–Air Bragg Mirrors *IEEE J. of Selected Topics in Quantum* Electronics **5** 111

[8] Garrigues M, Danglot J, Leclercq J-L and Parillaud O 2005 Tunable High-Finesse InP/Air MOEMS Filter *IEEE Photonics Technology Letters* **17** 1471

[9] Kusserow T, Zamora R, Sonksen J, Dharmarasu N, Hillmer H, Nakamura T, Hayakawa T and Vengatesan B 2008 Monolithic Integration of a Tunable Photodetector Based on InP/air-gap Fabry-Perot Filters *Proc. IEEE/LEOS Int. Conf. on Optical MEMS and Nanophotonics (Freiburg, Germany, 11-14 August 2008)* pp 134-135

[10] Irmer S, Alex K, Daleiden J, Kommallein I, Oliveira M, Römer F, Tarraf A and Hillmer H 2005 Surface micromachined optical low-cost all-air-gap filters based on stress-optimized Si3N4 layers *J. Micromech. Microeng.* **15** 867-872

[11] Lammel G, Schweizer S, Schiesser S and Renaud P 2002 Tunable Optical Filter of Porous Silicon as Key Component for a MEMS Spectrometer *J. Microelectromechanical Systems* **11** 815-827

[12] Saito M, Yamada I, Mizuta T, Matsuura A, Kawashima H, Sakaki A, Otsuka N, Shindo Y and Kuwabara T 2008 Tunable infrared filter made of thin silicon wedges *Infrared Physics & Technology* **51** 236–241

[13] Kasap S and Capper P 2006 *Springer Handbook of Electronic and Photonic Materials, Chapt. 21* (Springer) p 441

[14] Hearn E J 1977 (1997) *Mechanics of Materials 2, 3rd edition, Chapt. 7* (Oxford, UK: Butterworth-Heinemann) p 194